Soft Matter

PAPER

View Article Online
View Journal | View Issue

Cite this: *Soft Matter*, 2026, **22**, 343

Following the structural changes of triolein films during lipolysis

Ben A. Humphreys, *[abc] Philipp Gutfreund, [c] Andrew R. McCluskey, [def] Thomas Arnold, [gh] Jesper Vind[i] and Tommy Nylander [abjk]

Received 11th August 2025,
Accepted 18th November 2025

DOI: 10.1039/d5sm00820d

rsc.li/soft-matter-journal

A major challenge hampering the industrial and biological exploitation of lipases is the self-limiting effect of the lipolytic reaction. Defying sustained attention throughout history, the influence of lipase catalysed lipolysis on the internal structure of thin triglyceride films has proved elusive. An in-depth understanding of the lipolysis process at the triglycerides/aqueous interface will assist in creating innovative methods to enhance yields. This study furthers our understanding of the influence of solution pD (pH equivalent for aqueous solutions prepared with D_2O) on the effect of lipolysis on the structure of thin triolein films. All experiments were performed at pD 7.0 or pD 8.5, either side of the apparent pK_a of the primary product of the hydrolysis (oleic acid/oleate). Spectroscopic ellipsometry measurements were employed to kinetically track the changes in thickness of the triolein film after the introduction of 2 ppm *Thermomyces lanuginosus* lipase (TLL). Neutron reflectometry experiments revealed the internal structure of the thin films before and after TLL digestion, while fast kinetic measurements capturing changes to the reflectivity profile throughout lipolysis. Both techniques revealed significant variations in the physical properties and enzymatic conversion of the triolein films between pD 7.0 and pD 8.5.

Introduction

While it is well known that triglycerides are an essential dietary requirement, they are also utilised in industrial and biological processes such as pharmaceutical manufacturing and food formulations.[1–3] Common throughout biological and industrial triglyceride processes is the presence of an aqueous environment. Whilst there has been significant advances throughout history in the study of aqueous/lipid systems, such as changes in the liquid crystalline phase structure during lipolysis, there are still many questions left unanswered.[1,2,4–13] Although the physicochemical properties of the oil/water interface and how they change during lipolysis have recently been investigated, probing the influence of lipase catalysed lipolysis on the internal structure of a thin triglyceride film has proved elusive.[12–15] Consequently, studying how the structural changes within a planar, nanosized triolein film upon exposure to a lipolytic enzyme in an aqueous environment is of fundamental importance.

Lipases are an exceptional type of aqueous soluble enzyme that are highly active at interfaces such as that presented by an aqueous solvent in contact with a thin triolein film.[16,17] This phenomenon, referred to as interfacial activation was first reported by Sarda and Desnuelle in 1958,[18] and has since been extensively studied with its origins found to be directly related to the molecular orientation of the lipase binding site adjacent to an interface, which triggers a conformational "lid opening" change in the lipase structure.[17,19–24] Furthermore, lipolysis is often associated with a lag phase, where there is a period after the introduction of the enzyme before any significant activity is observed. The origins of this behaviour have been associated with slow adsorption of the lipase at the interface,[25] or the requirement of a certain amount of hydrolysis products to be present before optimal activity is observed.[26,27] The influence of hydrolysis products, has been further investigated where it was found that solution pH played a significant role on the lag phase duration.[12,15,28] While lipases such as those from

[a] *Physical Chemistry, Department of Chemistry, Lund University, P.O. Box 124, S-221 00 Lund, Sweden*
[b] *NanoLund, Lund University, SE-221 00 Lund, Sweden*
[c] *Institut Laue-Langevin, 71 Avenue des Martyrs, CS20156, 38042 Grenoble, France. E-mail: humphreys@ill.fr; Tel: +33 457428331*
[d] *Centre for Computational Chemistry, School of Chemistry, University of Bristol, Cantock's Close, Bristol BS8 1TS, UK*
[e] *European Spallation Source ERIC, Data Management and Software Centre, Asmussens Allé 305, DK-2800 Kongens Lyngby, Denmark*
[f] *Diamond Light Source, Harwell Campus, Didcot OX11 0DE, UK*
[g] *European Spallation Source ERIC, P.O. Box 176, SE-221 00 Lund, Sweden*
[h] *ISIS Pulsed Neutron and Muon Source, STFC, Harwell Science and Innovation Campus, OX11 OQX, UK*
[i] *Novonesis A/S, Biologiens Vej 2, 2800 Kgs. Lyngby, Denmark*
[j] *LINXS Institute of Advanced Neutron and X-ray Science, Mesongatan 4, 224 84 Lund, Sweden*
[k] *School of Chemical Engineering and Translational Nanobioscience Research Center, Sungkyunkwan University, Suwon, Republic of Korea*

Thermomyces lanuginosus, *Rhizopus delemar*, *Candida rugosa*, *Rhizomucur miehei*, and *Candida antarctica* A and B have gained significant industrial interest as biocatalysts,[17,29] a major challenge hampering the further industrial utilization of lipases is the self-limiting effect of the lipolytic reaction. While the reaction products such as free fatty acids, mono- and diglycerides are extremely useful in the food and cosmetic industry,[30,31] they are often poorly soluble or highly surface active themselves, therefore, impede enzymatic conversion.[12,23,32–36] An in-depth understanding of the lipolysis process at the triglycerides/aqueous interface will assist in creating innovative methods to enhance yields.

Thermomyces lanuginosus lipase (TLL) is a selective lipase that only attacks the Sn-1 and 3 positions of a triglyceride. However, the remaining monoglyceride (Sn-2) is kinetically less stable than the Sn-1,3 isomers, and will eventually undergo acyl migration leading to the complete triglyceride digestion.[37–39] Previous studies have shown that the pH of the aqueous TLL solution can influence the degree of digestion by controlling the protonation state of all species present as well as the surface charge at the oil/water interface.[12,15,23,28] Although the pK_a of monomeric fatty acids in approximately pH 4.8,[40] self-association, and a decrease in the local dielectric constant near the interface increases the apparent pK_a (pK_a^{app}) to 8–8.5 for longer chain fatty acids such as oleic acid.[41,42] The influence of pH on interfacial activity of regioselective lipases on triglycerides has been previously investigated.[23,34,35,43] However, this work used pendant drop tensiometric measurements, which give limited information regarding the structural changes of the triglyceride at the lipid/aqueous interface. Our study addresses this, by focusing on the influence of pH on the TLL digestion of a thin triolein film on a planar substrate.

This research makes use of neutron reflectometry (NR) and spectroscopic ellipsometry (SE) to reveal the physical and structural changes that occur at the triolein/aqueous interface. Herein, it was found that the influence of pH, and therefore the protonated state of the oleic acid product, has a significant impact on the internal structural changes and lipase activity.

Experimental

Our approach here is to use aqueous buffer solutions prepared with D_2O instead of H_2O for all experiments, as this is essential for the neutron reflectometry study due to the increased contrast between triolein and the solvent. While it is often assumed that there is no appreciable difference in system behaviour between H_2O and D_2O solutions, the use of D_2O for all experiments throughout this study unequivocally avoided any isotopic effects between the two techniques.[44] The triolein films were first exposed to buffer solutions at pD 7.0 or 8.5 (pH equivalent for aqueous solutions prepared with D_2O) until equilibration was achieved. The hydrated film was subsequently exposed to 2 ppm TLL after which the structural changes due to lipolysis were monitored for several hours using NR and SE. The pD values of 7.0 and 8.5 were chosen to be above the isoelectric point of TLL (pH 4.7),[45] but on either side of the pK_a^{app} of the oleic acid/oleate product. These results enabled detailed insight into pH effects on the changes to the internal structure as well as kinetics and enzymatic conversion throughout lipolysis. While this research is an extension on our previous studies, a significantly thinner triolein layer was employed for optimal NR measurements.

Materials

Polished, and thermally oxidized silicon wafers for ellipsometry were purchased from Siltronix, Archamps-France. Polished, silicon blocks with native oxide layer for neutron reflectometry were purchased from Siltronix, Archamps-France. HCl (37%), DCl (37%), H_2O_2 (30% (w/w)) and $CaCl_2{\cdot}2H_2O$ (>99%) were purchased from Merck. TRIS base (≥99.9%) was purchased from Sigma, and Honeywell Burdick and Jackson supplied NH_4OH (25%). Poly(styrene-d8) (dPS) 307 000 Da, PDI: 1.06, was purchased from Teknolab. The active wild type and inactive mutant *Thermomyces lanuginosus* lipase (TLL) were kindly provided by Novonesis (Denmark) at a concentration of 2500 ppm (see Fig. S1 in SI for molecular structure). TLL and triolein were stored at −20 °C until required. Toluene (99.8%) (from Sigma-Aldrich) and *n*-hexane (≥99%) (from Merck) were dried over 4 Å molecular sieves (Riedel-de Haën) for at least 1 day before use. Water obtained from a Milli-Q system (Merck Millipore, 18.2 MΩ cm at 25 °C) was used throughout. All reagents were used as received unless stated otherwise. A deuterated buffer solution prepared with 100 mM TRIS base and 1 mM $CaCl_2$ in D_2O was used for all experiments with the pD adjusted to pD 7.0 or 8.5 using concentrated DCl. From here on, this will be referred to as pD 7.0 buffer or pD 8.5 buffer. The lipase solutions were prepared at a concentration of 2 ppm TLL in the deuterated buffer solution, which enabled the kinetics of the digestion to be slow enough to be followed throughout the experiments and is consistent with our previous results.[12,14] Buffer solutions were stored at 4 °C until required and used within 1 week of preparation. We have made the assumption that there should be no discernible difference between H_2O and D_2O solutions for this system therefore results should be comparable to previous studies in aqueous solutions.

Methods

Substrate preparation. The silicon wafers for SE and silicon blocks for NR were thoroughly cleaned before starting the experiments with a detailed protocol provided in the SI. A dPS layer was added to the cleaned silicon wafers or silicon blocks using a LabSpin Spin Coater (Suss Micro Tec Lithography GmbH) or Delta 6 RC TT spin coater (SÜSS MicroTec Lithography GmbH) respectively. The dPS layer was included to increase the stability of the meta-stable triolein film.[46] Here, dPS was used to increase the scattering length density (SLD) contrast between the dPS and triolein layers in the NR studies and used in the SE experiments for consistency between techniques. For the SE silicon wafers, 30 μL of 0.25 wt% dPS in toluene was rapidly syringed onto the substrate while spinning at 2000 RPM for 30 s. The triolein layer was then spin-

coated onto the dPS film by injecting a 30 μL of 0.25 wt% triolein in hexane while spinning at 2000 RPM for 30 s. For the NR silicon block preparation, the volume of each solution syringed onto the substrate was increased from 30 μL to 200 μL to account for the increased surface area with all other parameters in the protocol remaining the same. Preliminary tests using the LabSpin Spin Coater for the silicon block surface preparation confirmed that the SE measured thickness of the dPS layer was 102.2 ± 2.8 Å and triolein layer was 126.5 ± 8.4 Å, averaged from nine measurements across the 50 × 80 mm surface. Actual thickness of the triolein film prepared for the NR measurements may vary slightly from this as a different spin coater was used.

Spectroscopic ellipsometry (SE). A UVISEL spectroscopic ellipsometer (HORIBA Jobin Yvon) was used for dry and solvated SE measurements as discussed previously.[12] Data analysis to obtain the thickness for each of the substrates layers was performed using the refellips analysis package.[47] The refractive index values for the silicon, silica and dPS were obtained from the RefractiveIndex.INFO website while the optical properties of the triolein layer in air and buffer solution were previously determined,[12,14] and Cauchy's equation was applied for the solvated measurements to account for the wavelength dependence of the refractive index.

For *in situ* measurements, a custom-designed fluid cell with an internal volume of ∼4 mL and optical quartz windows (Hellma optics) fixed at 70° was used throughout.[12] This enabled SE measurements to be conducted in a horizontal orientation with the ability to exchange the solvent. The temperature of the fluid cell was controlled at 25 °C for all experiments. The hydration step involved flowing deuterated buffer solution through the SE cell using a peristaltic pump at 2.3 mL min^{-1} for 10 min. The film thickness was monitored until an equilibrium thickness was observed. A deuterated buffer solution with 2 ppm TLL was then flowed through the cell at 2.3 mL min^{-1} for a further 10 min. A multilayer-slab model was utilized for the *in situ* SE experiments with the dry thickness values for silicon oxide and dPS (measured stepwise during surface preparation) fixed within this model. The lipid layer was modelled as a linear effective medium approximation (EMA) layer of triolein and buffer solution of unknown thickness and composition below an ambient buffer layer. This model provided a solvated triolein thickness, averaged over the size of the measurement spot. While SE was able to capture the trends in the changes in triolein film thickness over time, the internal structural inhomogeneity of the film was not considered, therefore, the SE modelling will not be as accurate as the analysis performed on the neutron reflectometry measurements.

Neutron reflectometry (NR). NR experiments were performed on FIGARO,[48] the horizontal time-of-flight reflectometer at the Institut Laue-Langevin (ILL), Grenoble, France, where a polychromatic beam with a wavelength range 2 Å < λ < 20 Å was exploited. All measurements were performed on a 50 × 80 × 15 mm silicon block housed in temperature controlled solid/liquid cell at a fixed temperature of 25 °C. Two incident angles, θ_i = 0.632° and θ_i = 3.766° were selected to access the momentum transfer range 0.007 $Å^{-1} < Q_z < 0.4$ $Å^{-1}$. The instrument was configured to provide a $\Delta Q/Q$ resolution of approximately 4.2%. The detector, which allows the off-specular scattering (OSS) and the specular reflectivity (SR) to be measured simultaneously, has a resolution of 2.2 × 4.8 mm^2 (FWHM) and a size of 30 × 47 cm^2 at a distance of 2.8 m from the sample. The beam footprint (defined by collimation slits) on the sample was set to 35 × 65 mm^2 for both reflection angles. In neutron SR, the reflectivity, R, is measured as a function of the angle of incidence θ, or momentum transfer $Q_z = (4\pi \sin\theta)/\lambda$, where λ is the wavelength of the neutron beam. The reflectivity is dependent on the nature of the interface, and especially on the coherent neutron scattering length density (SLD) of the materials, which is defined as the sum of the coherent scattering lengths of all atoms in a molecule divided by the molecular volume. The thickness of adsorbed layers and roughness of the interfaces also determine the reflectivity. By modelling the structure of the reflecting surface as a series of layers corresponding to the molecular constituents, it is possible to determine the composition and the one-dimensional structure (*i.e.*, normal to the substrate).

The raw NR data was normalised to the incident beam spectrum by the data reduction software COSMOS and modelled using the refnx software package (see SI for the Jupyter Notebooks used for the modelling).[49] We employ a model for each system comprised of a series of slabs. These components contain parameters regarding the respective thickness, roughness, and SLD of each layer. From ''fronting'' to ''backing'', the model structure contained slabs for the silicon, silicon oxide, dPS, three or four triolein/product layers, and solvent. Several other models were tested throughout the analysis of the NR results, including simpler options with less slab layers for the triolein film, or more complex options incorporating dual models with slabs and an exponential decay, or the use of multiple splines. For reference, modelled fits and SLD profiles for these alternative options are provided in the SI (see Fig. S2–S8). The model chosen for each system was the simplest option that provide an adequate fit. For each system (pD 7.0 or pD 8.5), the initial and final measurements were co-refined with the silicon, silicon oxide, dPS, and solvent parameters linked between the models as these values should be unaffected by the reaction. The SLD of the triolein/product layers were allowed to vary between 0.1 × 10^{-6} $Å^{-2}$, (pure triolein) and 6.36 × 10^{-6} $Å^{-2}$ (pure D_2O solvent) to account for varying degrees of solvent penetration. The models produced an SLD profile perpendicular to the substrate which was then used to calculate the corresponding reflectivity profile *via* the Abeles matrix method.[50] This calculated reflectivity profile can then be directly compared to the measured reflectivity profile to determine the quality of the model/fit.

Because the neutron reflectivity spectra were recorded using a two-dimensional detector, the off-specular neutron reflectivity (OSS) was also accessible. The intensity of the OSS is dependent on neutrons scattered away from the mirror reflection. When OSS is observed, the total momentum transfer also possesses an in-plane component. This allows one to determine SLD

variations parallel to the interface, but due to the geometry, the momentum transfers are typically two orders of magnitude smaller than in SR and, therefore, the spatial resolution is much lower, probing micrometre- instead on nanometre-sized structures.[51] Herein, the 2D OSS patterns were simulated in wavelength *vs.* scattering angle space using the distorted wave born approximation (DWBA).[52] This gave access to one additional parameter, namely, the mean size of in-plane inhomogeneities. One obvious sign of OSS from a surface, is the lack of total SR below the critical angle. This is clearly observed for our initial measurement at pD 7.0 and is discussed in the results and discussion section. However, the lack of total reflectivity due to OSS complicates the SR analysis therefore, a reduced Q range, only including data points beyond the critical angle was utilised in the modelling for this system with the scale factor assumed to be 1.

Akin to SR analysis, many different models can provide good fits for OSS and one must consider the validity of the model to determine if the results are realistic. For reference, an alternative OSS model for the pD 7.0 digested film is provided in the SI (see Fig. S9). While this model provides an equally good fit for the OSS to the chosen model provided herein, the structure that it describes was deemed unfeasible due to the excessive amount of TLL required.

Results and discussion

Table 1 reports the dry thicknesses for the silicon oxide, dPS, and triolein layers as well as the solvated triolein thickness at equilibrium after exposure to the buffer solutions for the SE investigation. Four separate experiments were performed in this study, with the active TLL directly compared with an inactive mutant variant of the enzyme (more than 1000 times less active) at both pD 7.0 and pD 8.5. The dry thicknesses for dPS and triolein presented in Table 1 highlight the reproducibility of the protocol used in the surface preparation with the standard deviation between each sample being less than 2% of the average thickness for dPS layers and 3% of the average thickness for the triolein films. The solvated triolein thicknesses reveal the first major difference between pD 7.0 and pD 8.5 conditions. While the increase in thickness is quite comparable at the same pD (for both active and inactive TLL experiments), the solvated triolein films at pD 8.5 were significantly thicker compared to pD 7.0. It must be noted that our previous investigation of this system did not see this behaviour,[12] however, we believe that this disparity is due to the difference in surface preparation, specifically relating to the thickness of the triolein layer. The origin of this difference in thickness as a function of pD requires further investigation that is beyond the scope of this work. However, we hypothesise that the small amount of oleic acid naturally present in the triolein film exposed to aqueous buffer, has a relatively much greater impact on the equilibrated thickness for the thinner triolein films investigated here. As previously reported, the oleic acid should be present predominantly as protonated, neutral species at pD 7.0 and as deprotonated, negatively charged oleate species at pD 8.5.[12] Therefore, the accumulation of negative charges within the triolein film should cause internal repulsion between other oleate moieties, as well as the underlying silicon oxide layer, which would lead to the significantly thicker solvated layers observed here. This hypothesis is supported by a recent study by Frigerio *et al.* which found, *via* confocal Raman microscopy and NMR, that TRIS moieties were detected at the triolein/aqueous interface at pH 9.0.[13] They proposed that the protonated TRIS species, influenced by the local pH environment, formed a cationic counter-ion to the negatively charged oleate. Given that the current investigation was performed at a lower pD of 8.5, we would expect that the amount of TRIS present in the protonated state would be larger and therefore the likelihood of forming TRIS/oleate ion pairs at the interface will be increased. After the triolein films reached an equilibrated thickness (no appreciable change for a minimum of 10 minutes), 2 ppm of the active or mutant TLL was introduced into the cell. Fig. 1 presents the changes in thickness of the four films throughout 30 minutes of lipolysis. Firstly, it is evident that the mutant TLL (black dashed lines in Fig. 1A and B) had no impact on the overall film thickness within 30 minutes, independent of the solution pD. This is an important discovery as it rules out any specific TLL effects such as surface adsorption or triolein displacement/rearrangement from playing a role in the changes observed for the active lipase systems.

Focusing now on the active TLL experiment at pD 7.0 (presented as the green data in Fig. 1A), there was an initial increase in thickness observed over the first 5 minutes. We interpret this as the lag phase; a previously observed phenomenon for this system, where the TLL builds up at the aqueous/triolein interface before optimal conditions are met.[12] This lag phase ($\sim$6 minutes) was followed by a significant decrease in the triolein film thickness before steady-state equilibrium was achieved after $\sim$20 minutes. Our interpretation here is that the digestion products constantly rearrange into their preferred aqueous/lipid phases throughout this period, as discussed in a recent GISAXS study by Freire *et al.* on a similar system.[13] Starting from a relatively featureless broad peak from the disordered core–shell clusters of triolein,[53] they observed the formation of an L_2 phase followed by the possible emergence of a micellar cubic $Fd3m$ phase.

While TLL is a selective lipase, specifically targeting the Sn-1 and 3 positions of triolein, the remaining Sn-2 monoolein is

Table 1 Summary of dry thicknesses for silicon oxide, dPS, and triolein film layers as well as the buffer solvated triolein film at equilibrium before TLL exposure measured *via* spectroscopic ellipsometry. Parameter uncertainty is defined by the square root of the covariance matrix diagonal (further details can be found here[47])

Samples for SE experiments					
Experimental conditions		Silicon oxide (Å)	dPS (Å)	Dry triolein (Å)	Solvated triolein (Å)
pD 7.0	Active TLL	232 ± 1	196 ± 2	127 ± 17	558 ± 18
	Mutant TLL	156 ± 1	202 ± 1	121 ± 6	681 ± 7
pD 8.5	Active TLL	217 ± 1	194 ± 1	121 ± 3	1128 ± 13
	Mutant TLL	251 ± 1	194 ± 1	123 ± 16	1058 ± 13

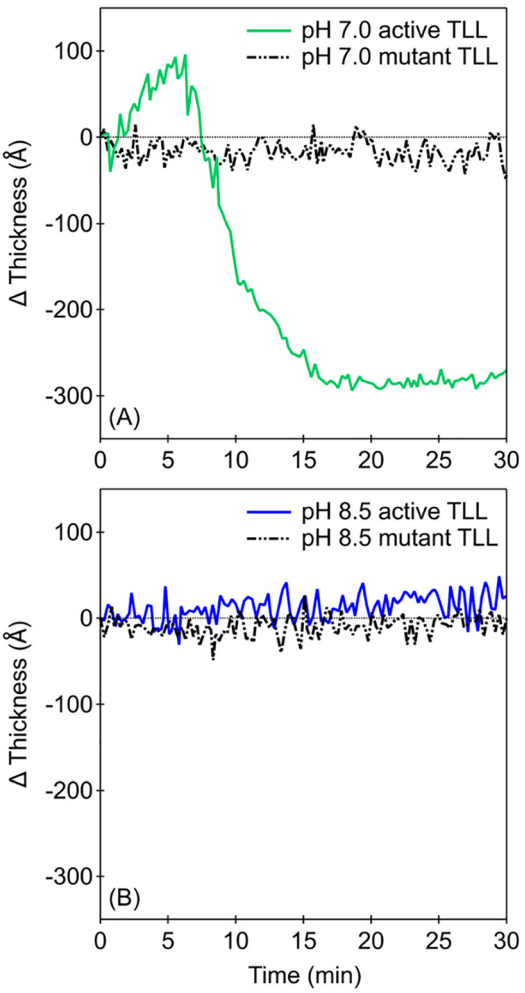

Fig. 1 Changes in thickness over time for (A) pD 7.0 buffer equilibrated triolein film with active TLL (solid green line) and mutant TLL (dashed black line) and (B) pD 8.5 buffer equilibrated triolein film with active TLL (solid blue line) and mutant TLL (dashed black line) measured by spectroscopic ellipsometry.

inherently unstable and through acyl migration, enables the complete lipolysis of the triolein film into oleic acid and the highly water-soluble glycerol.[9,12,37,39] We therefore interpret our observations as firstly, the oleic acid product, which favours the protonated, uncharged state at pH 7.0,[54] initially partitioning into the bulk oil phase adjacent to the dPS substrate.[13] However, as the amount of oleic acid exceeds a critical concentration, phase separation and de-wetting lead to loss of material from the oil phase into the aqueous environment resulting in the subsequent reduction in film thickness.

The behaviour of the system with the active TLL at pD 8.5 (blue data in Fig. 1B) was starkly different to that observed at pD 7.0. Here, we found no appreciable change in thickness throughout the 30 minutes of active TLL exposure.

While our previous investigation revealed an initial reduction in the film thickness, although much less than the corresponding pH 7.0 experiment, this study was performed on a significantly thicker triolein film, therefore, not directly comparable to this study.[12] We have previously proposed that the small amount of oleate originally present in the triolein film, in addition to any further oleate ions produced upon lipase addition, formed a uni- and bi-dentate calcium oleate complex barrier at the aqueous/triolein interface. However, as mentioned above, recent work by Frigerio *et al.*[13] revealed the presence of TRIS/oleate ion pairs at the aqueous/triolein interface which could also be responsible for hindering further hydrolysis and reducing the ability of products to transition into the aqueous phase.

The neutron reflectivity profile for the initial pD 7.0 measurement, before the introduction of active TLL is presented in Fig. 2(A). The measurement was performed on the buffer equilibrated triolein film and is equivalent to time = 0 in

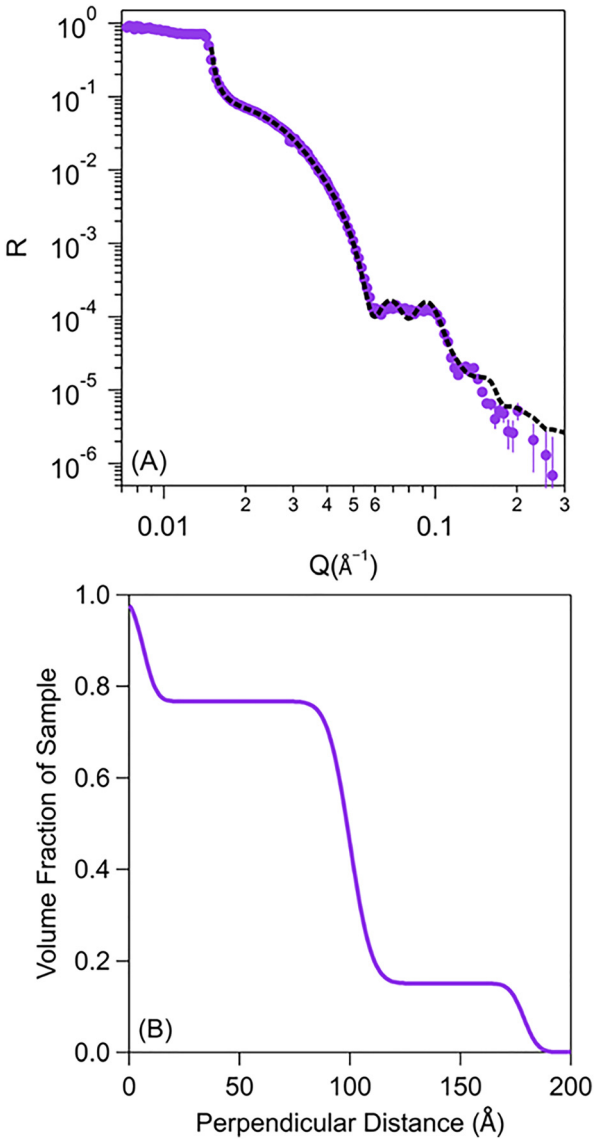

Fig. 2 (A) Measured reflectivity profile (closed circles) for the initial triolein film with fit (dashed black line) at pD 7.0. (B) Corresponding VFP profile displaying the fraction of sample within the thin film as a function of perpendicular distance normal to the dPS interface.

the ellipsometry results provided in Fig. 1(A). The SR fit presented as a dashed black line in Fig. 2(A) and corresponding volume fraction profile (VFP) shown in Fig. 2(B) were calculated from the modelled SLD profile provided in the SI (Fig. S10). The model employed for this system utilised three slabs for the triolein film, where each slabs thickness and solvent content was allowed to vary. As previously discussed in the in the experimental section for NR, alternative models were initially investigated. These preliminary tests revealed that a relatively complex model, here, three slabs for the triolein film, was required before an acceptable fit could be achieved. The results from the fitting process can be clearly visualised in the VFP provided in Fig. 2(B) where a very thin (<10 Å) pure triolein layer at the dPS interface is followed by two comparatively thicker layers (~90 Å each) with ~25% and ~80% solvent respectively. The Q-range for the data points utilised in the fitting process was restricted to $Q_z > 0.015$ Å^{-1} due to the presence of significant OSS. The OSS is responsible for the loss in SR intensity at low Q, where total reflection should be observed for this system. The VFP in Fig. 2(B) provides significantly more information about the structure of the buffer equilibrated triolein film normal to the substrate then simply the overall thickness provided in the SE results (Table 1). While the SE results are modelled using a single homogenous slab of solvated triolein, the SR analysis revealed that the degree of solvation is much greater at the aqueous/triolein interface (~80%) and progressively decreases to a layer of unsolvated, pure triolein at the dPS substrate. This large variation in triolein solvation throughout the film was unexpected for such a thin film where it was predicted that aqueous solvent would equally disperse throughout the triolein layer preferring the more hydrophilic ester regions of the triolein molecules. However, as neutron SR only provides information about homogenous layers within the thin film normal to the substrate, this interpretation could be misleading as in-plane heterogeneity is not considered.

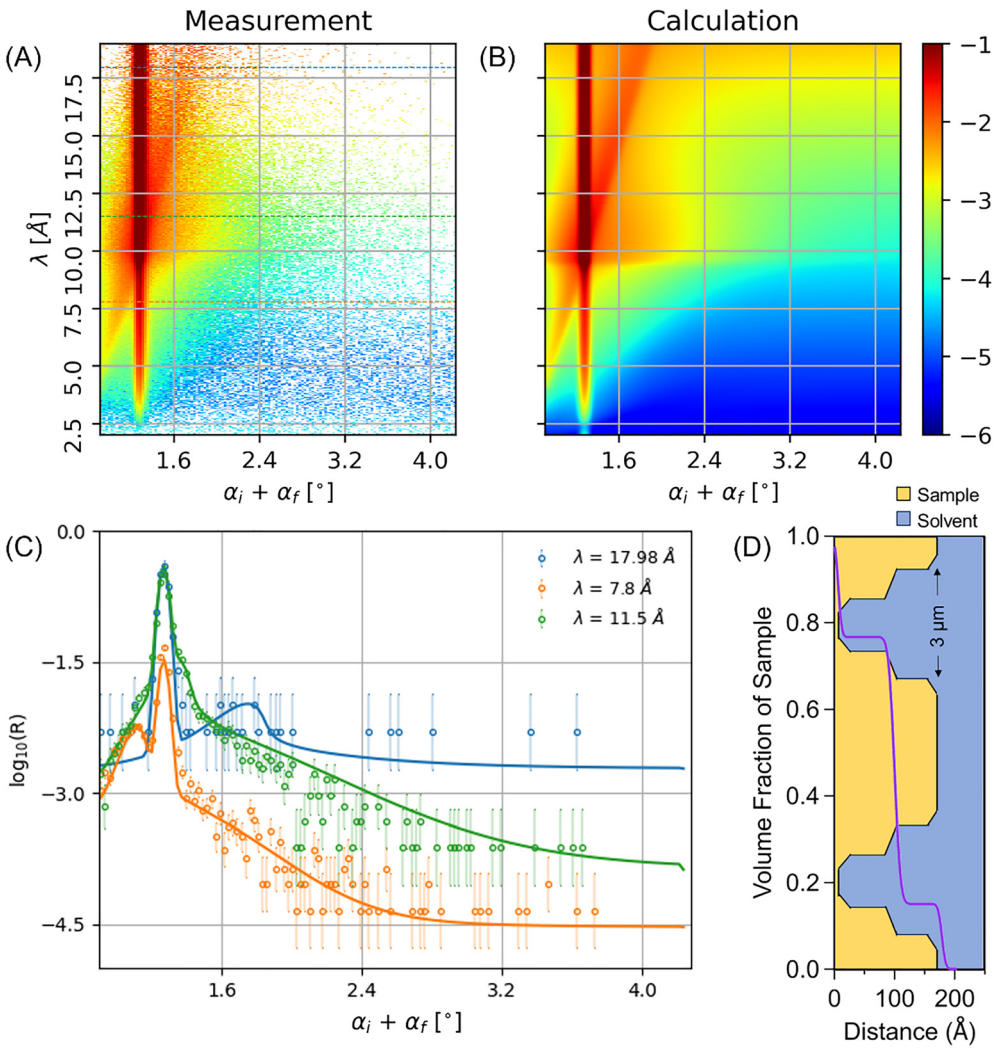

Fig. 3 (A) Measurement and (B) DWBA calculation (logarithmic colour scale) for the initial sample before TLL exposure in ($\alpha_i + \alpha_f$, λ) space. (C) The corresponding 1D cuts at different wavelengths indicated in the legend. (D) The VFP of the sample from the neutron SR analysis (purple line) overlaying a schematic diagram of the OSS model. Schematic diagram presented to highlight key characteristics of the film and is not to scale.

Complementary OSS modelling of the NR data was advantageous for the initial pD 7.0 measurement as it interrogated the SLD variations parallel to the interface with the analysis of the OSS provided in Fig. 3. The OSS for the NR data was analysed using recent advances in this field, highlighted in the work of Hafner *et al.*[52] The measured NR data is presented in Fig. 3(A) as λ *vs.* $\alpha_i + \alpha_f$ where α_i and α_f are the incident and outgoing glancing angles and λ is the neutron wavelength.

Presenting the date in this manner clearly highlights the presence of the off-specular scattering with a diagonal stripe of increased neutron intensity from bottom-left to top-right crossing the vertical specular reflection. Fig. 3(B) is the DWBA simulated plot, of a film consisting of, on average, 3 μm large conical-shaped, water-filled holes penetrating into the triolein layer. The corresponding 1D cuts at different wavelengths (blue, green and orange dashed lines in Fig. 3(A)) with fits from the calculation are provided in Fig. 3(C). The image created in the simulation (Fig. 3(B)) along with the quality of the fits in Fig. 3(C) indicate that the model is a good representation for this system. Finally, Fig. 3(D) presents a cartoon representation of the OSS analysis showing the conical protrusions of aqueous solvent (blue) penetrating into the triolein layer (yellow) overlaying the VFP for the triolein film from the SR analysis (purple line).

It is evident here that the volume fraction of solvent from the SR analysis, closely follows the penetration of the conical-shaped solvent protrusions predicted from the OSS calculations. This OSS analysis provides meaningful insight into the physical structure of the buffer equilibrated triolein film. While the initial interpretation of the VFP from the SR analysis implied an unexpected variation in the degree of triolein solvation normal to the substrate, we can now re-evaluate the VFP, incorporating the additional in-plane structural information from the OSS analysis. The combination of SR and OSS analysis provides, perhaps, a more realistic interpretation of the observed data, where the conical-shaped solvent protrusions are the origin of the projected solvent variation throughout the triolein film.

Following the buffer equilibrated film measurements, 2 ppm TLL solution was pumped through the solid/liquid cell at 1 mL min^{-1} for 15 minutes. The final NR measurement (Fig. 4(A)) was recorded four hours after TLL exposure to ensure complete hydrolysis of the triolein film. Our previous work confirms that triolein is completely digested under these conditions, therefore, the remaining products should be oleic acid which we expect to remain at the interface and the highly soluble glycerol which we expect to be removed.[12] The SR fit, presented as a dashed black line in Fig. 4(A) and corresponding VFP shown in Fig. 4(B) were calculated from the SLD profile provided in the SI (Fig. S10). Because total reflection at low Q was recovered ($R = 1$ at $Q_z < 0.014$ $Å^{-1}$), the influence of any OSS was significantly reduced, and the entire measured Q range was utilised in the fitting process. The model employed for the final digested system utilised two slabs to simulate oleic acid, separated by a thin layer of solvent. The thickness of each layer was allowed to vary, as well as the solvent content within the

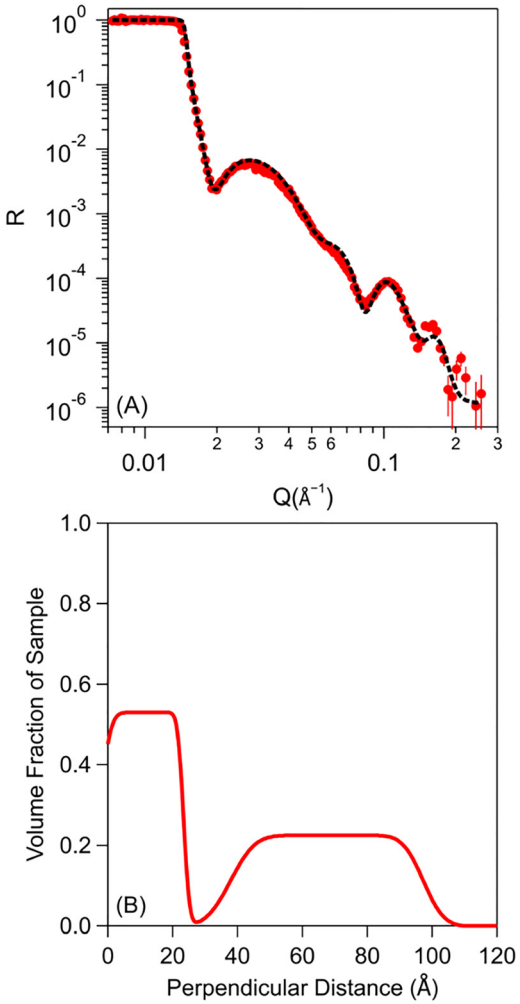

Fig. 4 Measured reflectivity profile (closed circles) for the final film four hours after the introduction of TLL with fit (dashed black line) at pD 7.0. (B) Corresponding VFP profile displaying the fraction of sample within the thin film as a function of perpendicular distance normal to the dPS interface.

two product slabs. The results from the SR fit can be visualised in the VFP provided in Fig. 4(B) where a ~20 Å interior layer of oleic acid with ~50% solvent content is located adjacent to the dPS interface, followed by a pure solvent layer (~10 Å) and a final oleic acid layer (~50 Å) with ~80% solvent. This physical interpretation of the VFP could, however, once again be misleading, as in-plane heterogeneity is not considered.

The OSS for the final pD 7.0 measurement was also analysed with the results presented in Fig. 5. The measured NR data is presented in Fig. 5(A) as λ *vs.* $\alpha_i + \alpha_f$ where the characteristic OSS diagonal stripe of increased neutron intensity crossing the vertical specular reflection from bottom left to top right was once again present, however, much lower in intensity compared to the initial measurement before TLL exposure. Fig. 5(B) is the corresponding DWBA simulation which assumes a film consisting of 2 μm aggregates floating on top of a thin product layer at the dPS interface, which is perforated with 10 μm solvent-filled holes. The corresponding 1D cuts at different wavelengths (blue, green and orange dashed lines in Fig. 5(A)) with fits from the

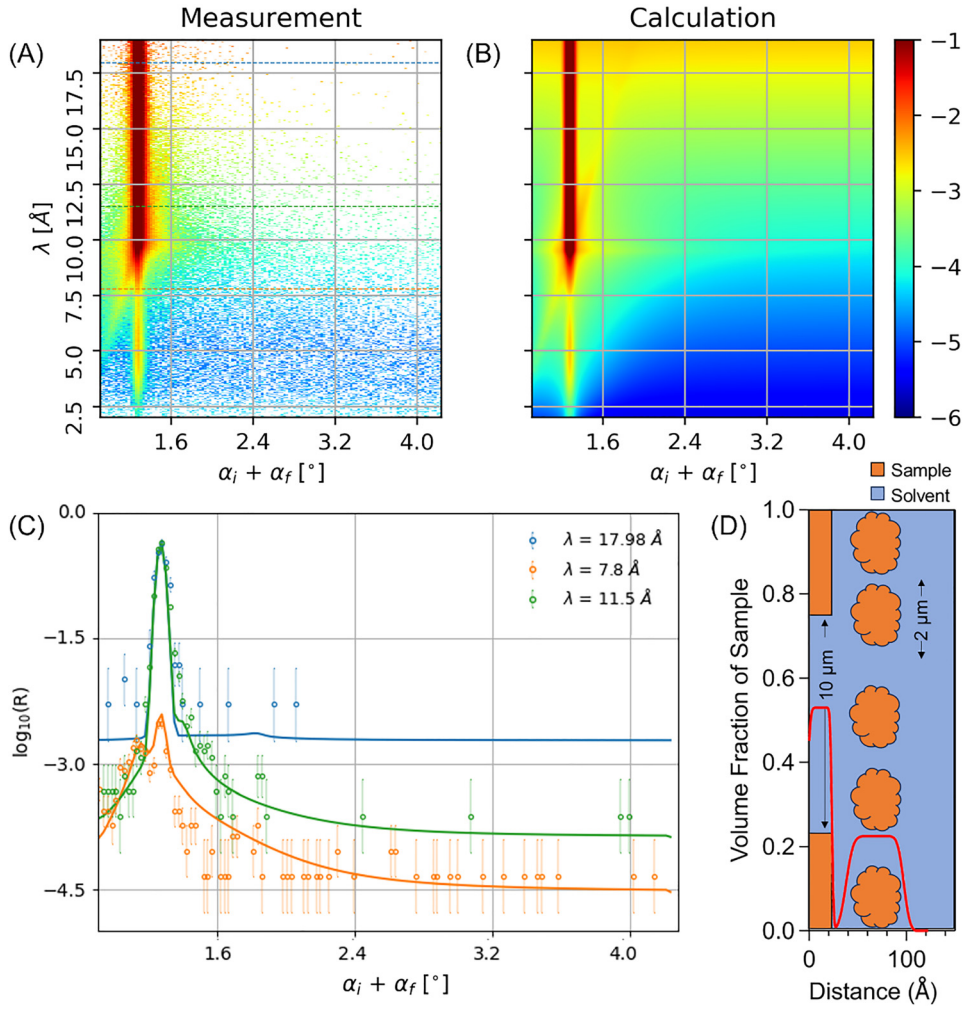

Fig. 5 (A) Measurement and (B) DWBA calculation (logarithmic colour scale) for the final sample after 4 hours of TLL exposure in ($\alpha_i + \alpha_f$, λ) space. (C) The corresponding 1D cuts at different wavelengths indicated in the legend. (D) The VFP of the sample from the specular NR analysis (red line) overlaying a schematic diagram of the model. Schematic diagram presented to highlight key characteristics of the film and is not to scale.

DWBA calculation are provided in Fig. 5(C). The simulated OSS is once again, in good agreement with the measured data, emphasised by the accuracy of the fits, indicating a high probability that this is a representative model for this system. Finally, Fig. 5(D) presents a cartoon representation of the OSS analysis overlaying the VFP for the digested film from the SR analysis (red line).

Our interpretation of this data is, therefore, as follows. A thin mixed layer (orange) of hydrolysis products is adjacent to the dPS interface with significant regions of aqueous solvent (blue) penetrating through to the dPS substrate with a floating layer of lipid aggregates suspended above. The composition of these lipid layers is not straight forward to determine. However, we would expect that both the oleic acid and monoolein can take up nearly 50% water as indicated by their phase behaviour.[2,5,42] Importantly, the volume fraction of solvent (red line) closely follows the degree at which the OSS calculations predict solvent is present at each layer.

The kinetics of the triolein lipolysis were followed using NR with measurements recorded every 30 seconds at a single angle, $\theta_i = 0.632^\circ$ covering the reduced Q range $0.007\ \text{Å}^{-1} < Q_z < 0.045\ \text{Å}^{-1}$. While this Q range is not adequate to properly fit a model, the results successfully reveal the gradual transition in the reflectivity profiles from the initial buffer equilibrated measurement, through to the final, completely digested measurement 4 hours after TLL exposure. Fig. 6 plots the condensed results for the kinetic NR measurements with individual 30 second measurements provided at 3-minute intervals for the first 30 minutes of lipolysis. Extended, higher temporal resolution plots for the kinetic measurements are provided in the SI (Fig. S11). Key findings from the kinetic measurements presented in Fig. 6 (and Fig. S11) are firstly, that the reflectivity profiles gradually transition from the initial to final equilibrium measurements within 30 minutes of lipolysis. The following 3.5 hours of measurements in the presence of 2 ppm TLL reveal no appreciable changes over the recorded Q range as shown in Fig. S12. Remarkably, the expected, total reflection below $Q = 0.014\ \text{Å}^{-1}$, is re-established within one minute (see Fig. S11(A)) indicating that the OSS is instantly

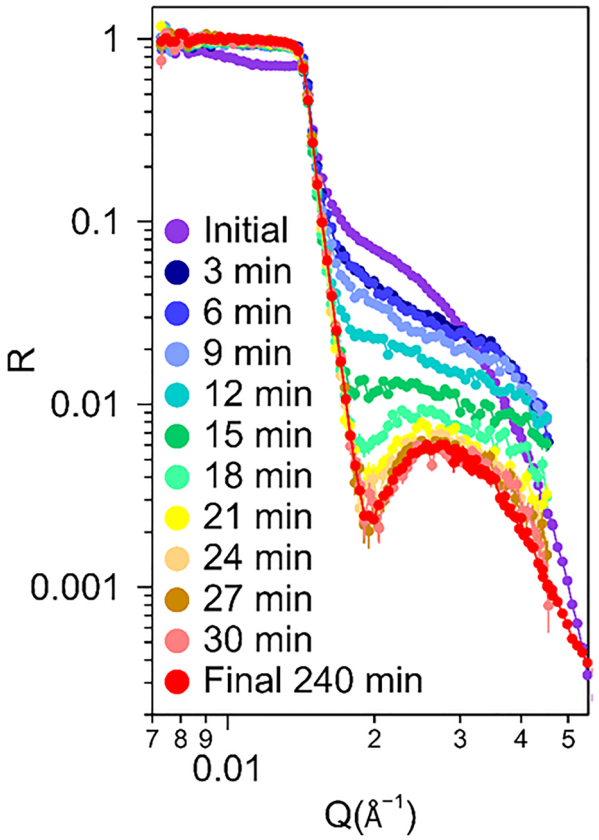

Fig. 6 Measured reflectivity profiles following the kinetics of the lipolysis of the triolein film after the introduction of 2 ppm TLL for 30 minutes (final measurement after 4 h). Lines to guide the eye.

reduced upon the addition of TLL. Here, we believe that the lipolytic products quickly build up at the aqueous/lipid interface and effectively fill the conical-shaped solvent protrusions responsible for the OSS in the initial buffer equilibrated measurement. However, it cannot be ruled out that the lipase molecules themselves also adsorb into these surface gaps.

Finally, the lag phase discussed in the ellipsometry results for the active TLL (Fig. 1(A)) is also observed in the NR kinetic measurements. The reflectivity profiles at the beginning of the triolein digestion are relatively static between the 1st and 6th minute (Fig. S11(A)) after the initial re-establishment of total reflection in reflectivity at low Q is observed. Our interpretation here is that, once the lipids/lipase build up at the aqueous/triolein interface, the TLL moieties must manoeuvre into the correct orientation to trigger the conformational ''lid-opening'' change in structure, leading to the active site of the enzyme being exposed to the triolein molecules.[17,19–24] Once in the correct orientation, the hydrolysis of triolein proceeded with subtle changes in the reflectivity profiles revealed between the 6th and 24th minute. The kinetic NR measurements reveal similar times for the important stages of the digestion process, such as lag phase and complete lipolysis equilibrium, as observed in the SE results presented in Fig. 1(A). Future advances in NR, will hopefully provide the ability to measure a wider Q range at this temporal resolution. This would enable the modelling of the reflectometry data and therefore, the ability to track the internal changes throughout the digestion process gaining a better understanding of the processes that are occurring. Enhanced lateral resolution could also be obtained by GISANS measurements.

NR profiles for the initial and final pD 8.5 measurements before and after the introduction of active TLL are presented in Fig. 7(A). The SR fits, presented as dashed black lines in Fig. 7(A) and corresponding VFP's shown in Fig. 7(B) were calculated from the modelled SLD profiles provided in the SI (Fig. S13). The SR modelling provided results that are in close agreement with the SE study presented in Table 1 and Fig. 1(B) with both techniques revealing a significantly thicker triolein film at pD 8.5 than at pD 7.0, with very little to no change observed after the introduction of active TLL. Fig. 7(C) plots the 30 second kinetic NR measurement of the enzymatic reaction at 1-minute intervals for the first 10 minutes of lipolysis. The kinetic measurements confirm that there is very little change in the NR profiles over this Q range after introducing TLL and the final equilibrated film is achieved within 10 minutes of lipolysis. The following 110 minutes of measurements reveal no appreciable changes over the recorded Q range as shown in Fig. S14. The fitted data suggests that the solvent content throughout the triolein film was significantly greater than at pD 7.0 which explains the notable increase in film thickness between the two conditions, while the complexity of the VFP's is likely a result of the additional lipid species present within the film. We suggest that small amount of charged oleate species are likely to be present as individual ions dispersed throughout the triolein film, as uni- and bi-dentate calcium oleate complexes or as a TRIS/oleate ion pair.

Focusing on the initial pD 8.5 buffer equilibrated measurement, the structure of the film was significantly more complex than the corresponding pD 7.0 film with four slabs now required for the triolein layer, before the SR model could adequately fit the NR profile. The thickness and solvent content of each triolein slab was allowed to vary throughout the fitting process. The results from the SR modelling can be visualised in the purple VFP provided in Fig. 7(B). Moving through the film perpendicularly from the dPS substrate to the pure solvent, we first see a thin, ~15 Å interior layer of triolein with ~30% solvent. We believe the thin inner region is likely to be pure triolein molecules strongly interacting with the dPS substrate, similar to the pD 7.0 case. This thin interior layer is followed by an ~80 Å thick, solvent rich layer (~80%). This second region is predicted to have a small percentage of oleate ions dispersed throughout the triolein molecules, drawing in aqueous solution to solvate the charged species and allow film expansion due to ion–ion and ion–substrate repulsion. A third region of ~50 Å thickness is then revealed with a significant reduction in solvent content (~50%). This third region of reduced solvation is harder to interpret but is potentially occupied by a small amount of calcium oleate complexes, *i.e.*, insoluble calcium soaps. This would explain the reduction in solvation within this region. However, previous studies propose that these calcium oleate complexes build up at the periphery of aqueous/triolein

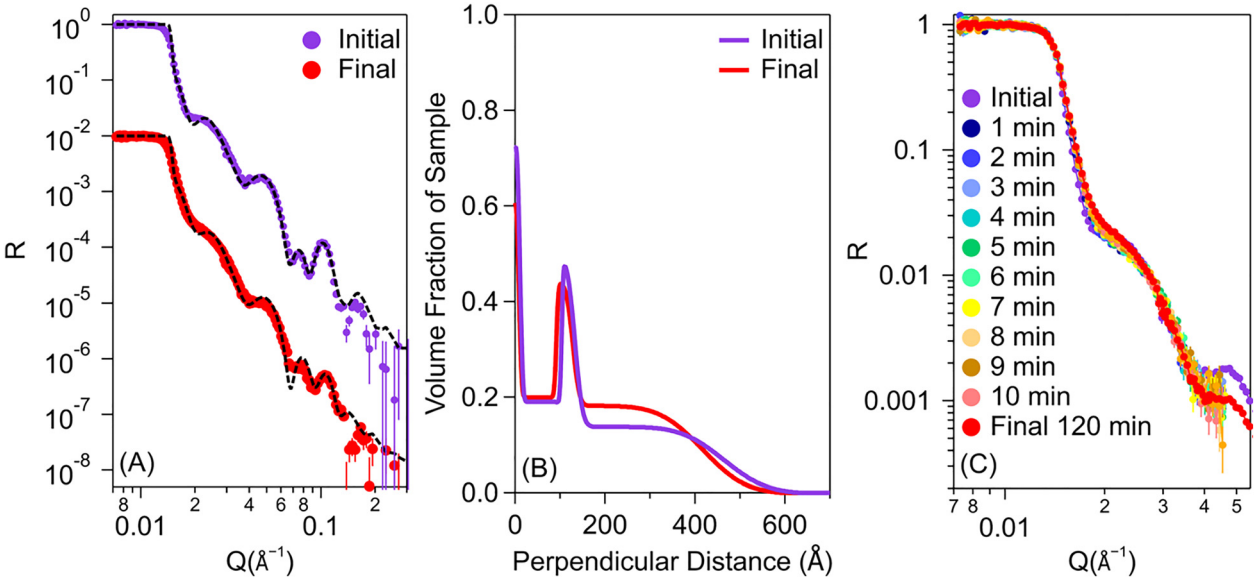

Fig. 7 (A) Measured reflectivity profiles (closed circles) for the initial triolein film (purple) and final product (red) with SR fits (dashed black lines) at pD 8.5. Data has been offset on the reflectivity axes for clarity, with the data for the initial triolein film plotted using actual recorded data. (B) Corresponding VFP profiles displaying the fraction of sample within the thin film as a function of perpendicular distance from the dPS interface. (C) Measured reflectivity profiles following the kinetics of the lipolysis of the triolein film after the introduction of 2 ppm TLL for 10 minutes (final measurements after 2 hours). Lines to guide the eye.

interface where they impede the interfacial biocatalysis, hinder the hydrolytic process, and drastically reduced the ability of the products to transition into the aqueous phase.[12,23] A final ~400 Å thick solvent rich (>80%) lipid layer is observed which gradually increases in solvent content until reaching the bulk. We hypothesize that this final region of the film has a build-up of TRIS/oleate ion pairs dispersed throughout the triolein molecules leading to significant solvent penetration to accommodate the ion charges and hydrophilic TRIS moieties, as well as the remarkably rough aqueous/triolein interface which was required in the SR modelling.

The red VFP for the final measurement in Fig. 7(B) is almost identical to the initial purple VFP providing further evidence that the lipolytic activity was drastically hindered. As previously discussed for the SE results, we conclude that the presence of uni- and bi-dentate calcium oleate complexes, and/or the TRIS/oleate ion pairs, form a barrier that significantly hinders triolein hydrolysis and reduce the ability of the products to transition into the aqueous phase.

Conclusions

This study expands on previous research on the lipolysis of triglyceride films through *in situ* characterisation of the structural changes of thin triolein films in TRIS buffer solutions at pD 7.0 and pD 8.5. Herein, we employ SE to determine changes in triolein film thickness after introducing TLL and compare the results to experiments performed in the presence of an inactive mutant TLL. NR measurements then probed the internal structure of the thin films before and after lipolysis with SR analysis providing information about the structure normal to the substrate while OSS analysis revealed the mean size of in-plane inhomogeneities. Fast NR measurements were also able to capture the kinetics of the reflectivity profiles changes throughout the film digestion. Both SE and NR found that solution pD significantly impacted the initial solvated triolein thickness and TLL digestion of the film. Upon introducing TLL at pD 7.0, an initial lag phase was observed before the film thickness decreased for ~20 minutes at which point film digestion was complete, *i.e.*, no further changes in SE thickness or NR profiles were observed. The combination of SR and OSS analysis reveals an initial triolein film with large conical shaped, water-filled holes penetrating into the triolein layer. After lipolysis, the internal structure of the film revealed aggregates of oleic acid and other lipolysis products floating on top of a perforated lipid layer at the dPS interface. At pD 8.5 however, the presence of negatively charged oleates, together with other lipids, caused the buffer equilibrated film to be significantly thicker than at pD 7.0 with a considerably more complex internal structure revealed. Remarkably, exposing the film to TLL at this pD had virtually no impact on film thickness or structure due to the presence of either calcium oleate complexes or TRIS–oleate ion pairs at the aqueous/triolein interface.

The findings from this study further our understanding of the digestion of thin triolein films and demonstrate how NR can reveal internal structural changes during lipolysis. Unfortunately, the Q range for our time-resolved measurements throughout the digestion was limited on the FIGARO beamline; a general problem for most existing neutron reflectometers. As a result, we were not able to effectively model the structural

changes occurring during digestion. The ability to measure over a wider Q-range with time resolution of around 30 s would have undoubtedly improved our understanding of this system. Increasing the neutron flux on the sample over a wider Q-range through redesign of the standard configuration for neutron reflectometers, or *via* a more powerful neutron source would go a long way towards realising this goal.

Author contributions

Ben Humphreys: conceptualisation, investigation, formal analysis, writing – original draft, Philipp Gutfreund: formal analysis, writing – review & editing, Andrew McCluskey: formal analysis, writing – review & editing, Thomas Arnold: conceptualisation, formal analysis, writing – review & editing, Jesper Vind: conceptualisation, writing – review & editing, Tommy Nylander: conceptualization, supervision, formal analysis, writing – review & editing.

Conflicts of interest

The authors declare that they have no known competing financial interests or personal relationships that could have appeared to influence the work reported in this paper.

Data availability

Supplementary information (SI): silicon wafer and silicon block cleaning protocol. The modelled SR SLD profiles for the pD 7.0 and 8.5 experiments before and after lipolysis. The measured reflectivity profiles for the kinetic NR study at pD 7.0 revealing the changes for the first 30 minutes at higher temporal resolution. The measured reflectivity profiles for the kinetic NR study at pD 7.0 from 30 to 240 minutes and pD 8.5 from 10 to 120 minutes. The print outs of the Jupyter Notebooks for the pD 7.0 and pD 8.5 modelling. See DOI: https://doi.org/10.1039/d5sm00820d. Neutron reflectometry proposal information and data for the FIGARO beamtime at the ILL can be found at https://doi.ill.fr/10.5291/ILL-DATA.9-13-1005.

Other data will be made available on request.

Acknowledgements

This paper is dedicated to the memory of Erich Sackmann. We are grateful for the financial support from Swedish Research Council (2018-05013), The Swedish Agency for Economic and Regional Growth through the European Regional Development Fund (Grant No 20307448) and the Skane Region as well as NanoLund, Lund University (p12-2012). We are grateful for the beam-time allocation at the ILL on FIGARO.[55] We also acknowledge support from the Partnership for Soft Condensed Matter (PSCM) at the ILL for access to surface and sample preparation equipment.

References

1 J. Borné, T. Nylander and A. Khan, *J. Phys. Chem. B*, 2002, **106**, 10492–10500.
2 J. Borné, T. Nylander and A. Khan, *Langmuir*, 2002, **18**, 8972–8981.
3 B. Freedman, E. H. Pryde and T. L. Mounts, *J. Am. Oil Chem. Soc.*, 1984, **61**, 1638–1643.
4 F. Caboi, J. Borné, T. Nylander, A. Khan, A. Svendsen and S. Patkar, *Colloids Surf., B*, 2002, **26**, 159–171.
5 J. Barauskas, H. Anderberg, A. Svendsen and T. Nylander, *Colloids Surf., B*, 2016, **137**, 50–59.
6 W. K. Fong, S. Salentinig, C. A. Prestidge, R. Mezzenga, A. Hawley and B. J. Boyd, *Langmuir*, 2014, **30**, 5373–5377.
7 S. Salentinig, L. Sagalowicz and O. Glatter, *Langmuir*, 2010, **26**, 11670–11679.
8 S. Salentinig, L. Sagalowicz, M. E. Leser, C. Tedeschi and O. Glatter, *Soft Matter*, 2011, **7**, 650–661.
9 S. Salentinig, S. Phan, A. Hawley and B. J. Boyd, *Angew. Chem., Int. Ed.*, 2015, **54**, 1600–1603.
10 M. Wadsäter, J. Barauskas, T. Nylander and F. Tiberg, *ACS Appl. Mater. Interfaces*, 2014, **6**, 7063–7069.
11 D. Warren, M. Anby, A. Hawley and B. Boyd, *Langmuir*, 2011, **27**, 9528–9534.
12 B. A. Humphreys, J. Campos-Terán, T. Arnold, L. Baunsgaard, J. Vind, C. Dicko and T. Nylander, *Front. Soft Matter*, 2022, **2**, 929104.
13 M. Frigerio, R. V. M. Freire, T. A. Soares, H. Amenitsch, M. E. Leser and S. Salentinig, *J. Colloid Interface Sci.*, 2024, **665**, 1091–1101.
14 A. Stamm, A. Svendsen, J. Skjold-Jørgensen, T. Vissing, I. Berts and T. Nylander, *Chem. Phys. Lipids*, 2018, **211**, 37–43.
15 T. Snabe and S. B. Petersen, *Chem. Phys. Lipids*, 2003, **125**, 69–82.
16 P. Fojan, P. H. Jonson, M. T. N. Petersen and S. B. Petersen, *Biochimie*, 2000, **82**, 1033–1041.
17 R. D. Schmid and R. Verger, *Angew. Chem., Int. Ed.*, 1998, **37**, 1608–1633.
18 L. Sarda and P. Desnuelle, *Biochim. Biophys. Acta*, 1958, **30**, 513–521.
19 A. M. Brzozowski, U. Derewenda, Z. S. Derewenda, G. G. Dodson, D. M. Lawson, J. P. Turkenburg, F. Bjorkling, B. Huge-Jensen, S. A. Patkar and L. Thim, *Nature*, 1991, **351**, 491–494.
20 A. M. Brzozowski, H. Savage, C. S. Verma, J. P. Turkenburg, D. M. Lawson, A. Svendsen and S. Patkar, *Biochemistry*, 2000, **39**, 15071–15082.
21 M. Martinelle, M. Holmquist and K. Hult, *Biochim. Biophys. Acta, Lipids Lipid Metab.*, 1995, **1258**, 272–276.
22 R. Verger, *Trends Biotechnol.*, 1997, **15**, 32–38.
23 M. Muth, S. Rothkötter, S. Paprosch, R. P. Schmid and K. Schnitzlein, *Colloids Surf., B*, 2017, **149**, 280–287.
24 N. Willems, M. Lelimousin, J. Skjold-Jørgensen, A. Svendsen and M. S. P. Sansom, *Chem. Phys. Lipids*, 2018, **211**, 4–15.
25 R. Verger, M. C. E. Mieras and G. H. de Haas, *J. Biol. Chem.*, 1973, **248**, 4023–4034.
26 L. K. Nielsen, J. Risbo, T. H. Callisen and T. Bjørnholm, *Biochim. Biophys. Acta, Biomembr.*, 1999, **1420**, 266–271.

27 T. Wieloch, B. Borgström, G. Pieroni, F. Pattus and R. Verger, *J. Biol. Chem.*, 1982, **257**, 11523–11528.
28 T. Snabe, M. T. Neves-Petersen and S. B. Petersen, *Chem. Phys. Lipids*, 2005, **133**, 37–49.
29 R. Fernandez-Lafuente, *J. Mol. Catal. B:Enzym.*, 2010, **62**, 197–212.
30 E. Boyle, J. B. German and J. Whelan, *Crit. Rev. Food Sci. Nutr.*, 1996, **36**, 785–805.
31 R. Intarakumhaeng, Z. Shi, A. Wanasathop, Q. C. Stella, K. S. Wei, P. B. Styczynski, C. Li, E. D. Smith and S. K. Li, *Int. J. Cosmet. Sci.*, 2018, **40**, 367–376.
32 P. Reis, H. Watzke, M. Leser, K. Holmberg and R. Miller, *Biophys. Chem.*, 2010, **147**, 93–103.
33 P. Reis, K. Holmberg, H. Watzke, M. E. Leser and R. Miller, *Adv. Colloid Interface Sci.*, 2009, **147–148**, 237–250.
34 P. Reis, R. Miller, M. Leser, H. Watzke, V. B. Fainerman and K. Holmberg, *Langmuir*, 2008, **24**, 5781–5786.
35 P. Reis, K. Holmberg, R. Miller, J. Krägel, D. O. Grigoriev, M. E. Leser and H. J. Watzke, *Langmuir*, 2008, **24**, 7400–7407.
36 P. Reis, T. W. Raab, J. Y. Chuat, M. E. Leser, R. Miller, H. J. Watzke and K. Holmberg, *Food Biophys.*, 2008, **3**, 370.
37 J. A. Laszlo, D. L. Compton and K. E. Vermillion, *J. Am. Oil Chem. Soc.*, 2008, **85**, 307–312.
38 S. Salentinig, N. R. Yepuri, A. Hawley, B. J. Boyd, E. Gilbert and T. A. Darwish, *Chem. Phys. Lipids*, 2015, **190**, 43–50.
39 S. Murgia, F. Caboi, M. Monduzzi, H. Ljusberg-Wahren and T. Nylander, *Prog. Colloid Polym. Sci.*, 2002, **120**, 41–46.
40 D. P. Cistola, D. M. Small and J. A. Hamilton, *J. Lipid Res.*, 1982, **23**, 795–799.
41 D. P. Cistola, J. A. Hamilton, D. Jackson and D. M. Small, *Biochemistry*, 1988, **27**, 1881–1888.
42 S. Mele, O. Söderman, H. Ljusberg-Wahrén, K. Thuresson, M. Monduzzi and T. Nylander, *Chem. Phys. Lipids*, 2018, **211**, 30–36.
43 P. Reis, K. Holmberg, R. Miller, M. E. Leser, T. Raab and H. J. Watzke, *C. R. Chim*, 2009, **12**, 163–170.
44 A. Krężel and W. Bal, *J. Inorg. Biochem.*, 2004, **98**, 161–166.
45 S. Barig, R. Alisch, S. Nieland, A. Wuttke, Y. Gräser, M. Huddar, K. Schnitzlein and K. Stahmann, *Eng. Life Sci.*, 2011, **11**, 387–394.
46 R. Vazquez, R. Nogueira, M. Orfão, J. L. Mata and B. Saramago, *J. Colloid Interface Sci.*, 2006, **299**, 274–282.
47 H. Robertson, I. J. Gresham, S. W. Prescott, G. B. Webber, E. J. Wanless and A. Nelson, *SoftwareX*, 2022, **20**, 101225.
48 R. A. Campbell, H. P. Wacklin, I. Sutton, R. Cubitt and G. Fragneto, *Eur. Phys. J. Plus*, 2011, **126**, 1–22.
49 A. R. J. Nelson and S. W. Prescott, *J. Appl. Crystallogr.*, 2019, **52**, 193–200.
50 A. Nelson, *J. Appl. Crystallogr.*, 2006, **39**, 273–276.
51 A. Hafner, P. Gutfreund, B. P. Toperverg, M. Geoghegan and M. Sferrazza, *J. Phys.: Condens. Matter*, 2021, **33**, 364002.
52 A. Hafner, P. Gutfreund, B. P. Toperverg, A. O. F. Jones, J. P. De Silva, A. Wildes, H. E. Fischer, M. Geoghegan and M. Sferrazza, *J. Appl. Crystallogr.*, 2021, **54**, 924–948.
53 A. Sadeghpour, M. L. Parada, J. Vieira, M. Povey and M. Rappolt, *J. Phys. Chem. B*, 2018, **122**, 10320–10329.
54 D. P. Cistola, J. A. Hamilton, D. Jackson and D. M. Small, *Biochemistry*, 1988, **27**, 1881–1888.
55 B. Humphreys, T. Arnold, A. Maestro and T. Nylander, *Institut Laue-Langevin (ILL)*, 2021, DOI: 10.5291/ILL-DATA.9-13-1005.